

Dual peaks evolving into single-peak for sub-wavelength 2-D atom localization in a V-type atomic system*

Shun-Cai Zhao ^{1, †} Xin Li,¹ and Ping Yang¹

¹*Department of Physics, Faculty of Science, Kunming University of Science and Technology, Kunming, 650500, PR China*

The atom localization of a V-type atomic system is discussed by the detunings associated with the probe and the two orthogonal standing-wave fields, and by the spontaneously generated coherence (SGC). Within the half-wavelength domain in the 2-dimensional(2-D) plane, the atom localization depicted by the probe dual absorption peaks is achieved when the detunings are tuned. However, the dual peaks change into single-peak when the SGC arises. The single-peak 2-D localization demonstrated the advantage for atom localization achieved by the flexible manipulating parameters in our scheme.

INTRODUCTION

Sub-wavelength atom localization becomes an active research topic from both the theoretical and experimental points of view[1, 2]. Several schemes based on the optical methods are introduced to measure the position of the atom, such as the spontaneous emission [3–5], absorption [6, 7], population [8–12], the entanglement between the atom's internal state and its position [13], the phase shift of the field[14] and gain [15]. In the schemes of an atom interacts with two orthogonal standing-wave fields [16–19], the atomic position information is given by multiple simultaneous quadrature measurement, the population in the upper state or in any ground state measurement, and incorporating the quantum interference phenomenon measurement, etc..

However, the implemented atom localization is multi-peak probe absorption in most of the optical methods[6, 7] or in the schemes of an atom interacts with two orthogonal standing-wave fields[16–19]. In our scheme, we analyzed the different parameters, i.e., the SGC and the detunings associated with the probe and two orthogonal standing-wave fields. The probe dual absorption peaks evolving into single-peak for the atom localization via the flexibly manip-

ulating manners is achieved by both the external fields and the quantum coherence, which demonstrates the advantage over the dual peaks atom localization schemes[16–19].

MODEL AND EQUATION

Let us consider a V-type system[see Fig.1] with the lower state $|1\rangle$ and two excited states $|2\rangle$ and $|3\rangle$. The transition $|1\rangle\leftrightarrow|3\rangle$ with frequency ω_{13} is driven by a weak probe field of frequency ν_p with Rabi frequency Ω_p being $\Omega_p=E_p\mu_{13}/2\hbar$. A strong coherent coupling standing-wave field $E_{x,y}$ with the same frequency ν_c is simultaneously applied to the transition $|1\rangle\leftrightarrow|2\rangle$ with frequency ω_{12} . The Rabi frequency $\Omega_c(x,y)$ corresponding to the composition of two orthogonal standing waves is $\Omega_c(x,y)=E_{x,y}\mu_{12}/2\hbar=\Omega_0[\sin(\kappa_1x+\delta)+\sin(\kappa_2y+\eta)]$. Where μ_{13} and μ_{12} are the corresponding dipole matrix elements, $\kappa_i=2\pi/\lambda_i$, ($i=1,2$) is the wave vector with wavelengths λ_i , ($i=1,2$) of the corresponding standing wave fields and the parameters δ and η are the phase shifts associated with the standing-wave fields. $\Delta_p=\omega_{13}-\nu_p$, and $\Delta_c=\omega_{12}-\nu_c$ are the detunings of the two corresponding fields, respectively. For simplicity, we assume Ω_p and Ω_0 to be real. $2\gamma_1$ and $2\gamma_2$ are the spontaneous decay rates

of the excited states $|2\rangle$ and $|3\rangle$ to the ground states $|1\rangle$, respectively. And in the atomic system, the two excited levels $|2\rangle$ and $|3\rangle$ are closely spaced such that the two transitions to the lower state interact with the same vacuum mode, SGC can be present. Which was proposed the realization in photonic band-gap materials and semiconductor quantum dots[20].

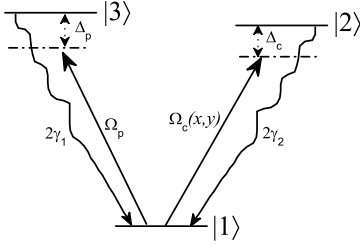


FIG. 1. Schematic diagrams. The position-dependent Rabi frequency $\Omega_c(x, y)$ corresponding to the atomic transition from $|2\rangle$ to $|1\rangle$. The transition from $|1\rangle$ to $|3\rangle$ is coupled via a weak probe field Ω_p . $2\gamma_1$ and $2\gamma_2$ are the atomic decay rates.

Here, the center-of-mass position distribution of the atom is assumed to be nearly uniform along the direction of the standing wave. Hence, we can apply the Raman-Nath approximation and ignore the kinetic energy of the atom in the Hamiltonian[21]. Then, under the electric dipole and rotating-wave approximation, the systematic density matrix in the interaction picture involving SGC can be written as[22],

$$\begin{aligned}
 \dot{\rho}_{22} &= -2\gamma_1\rho_{22} + i\Omega_c(\rho_{12} - \rho_{21}) - p\sqrt{\gamma_1\gamma_2}(\rho_{23} + \rho_{32}), \\
 \dot{\rho}_{33} &= -2\gamma_1\rho_{33} + i\Omega_p(\rho_{13} - \rho_{31}) - p\sqrt{\gamma_1\gamma_2}(\rho_{23} + \rho_{32}), \\
 \dot{\rho}_{12} &= -(\gamma_1 + i\Delta_c)\rho_{12} - p\sqrt{\gamma_1\gamma_2}\rho_{13} + i\Omega_c(\rho_{22} - \rho_{11}) \\
 &\quad + i\Omega_p\rho_{32}, \\
 \dot{\rho}_{13} &= -p\sqrt{\gamma_1\gamma_2}\rho_{12} - (\gamma_2 + i\Delta_p)\rho_{13} + i\Omega_c\rho_{23} + i\Omega_p \\
 &\quad (\rho_{33} - \rho_{11}), \\
 \dot{\rho}_{23} &= i\Omega_c\rho_{13} - i\Omega_p\rho_{21} - i(\Delta_p - \Delta_c)\rho_{23} - (\gamma_1 + \gamma_2)\rho_{23} \\
 &\quad - p\sqrt{\gamma_1\gamma_2}(\rho_{22} + \rho_{33}).
 \end{aligned} \tag{1}$$

The atom is initially in the ground state, therefore, we use the initial condition $\rho_{11}^0 = 1$, $\rho_{22}^0 = 0$, $\rho_{33}^0 = 0$ along with $\rho_{ij}^* = \rho_{ji}$. Here, the parameter p denotes the alignment of the two dipole moments and is defined as $p = \vec{\mu}_{13} \cdot \vec{\mu}_{12} / |\mu_{13}| |\mu_{12}| = \cos\theta$ with θ being the angle between the two dipole moments $\vec{\mu}_{12}$ and $\vec{\mu}_{13}$, which is very sensitive for the existence of SGC effect, and can be a random angle between 0 and 2π except for 0 and π . The terms with $p\sqrt{\gamma_1\gamma_2}$ represent the quantum interference resulting from the cross coupling between spontaneous emission paths $|1\rangle$ - $|2\rangle$ and $|1\rangle$ - $|3\rangle$. It should be noted that only for small energy spacing between the two excited levels are the interference terms in the systematic density matrix significant; otherwise the oscillatory terms will average out to zero and thereby SGC effect vanishes.

Because of the spatial-dependent atom-field interaction, 2-D atom localization can be realized via measuring the probe gain or absorption[15]. The information about the atomic position from the susceptibility[19] at the probe field frequency is what we want to get, and the nonlinear Raman susceptibility χ is then given by

$$\chi = \frac{2N|\mu_{13}|^2}{\epsilon_0\Omega_p\hbar}\rho_{13}, \tag{2}$$

where N is the atom number density in the medium and μ_{13} is the magnitude of the dipole-matrix element between

$|1\rangle$ and $|3\rangle$. ϵ_0 is the permittivity in free space. When the probe field is weak, i.e. $\Omega_p \ll \Omega_c$, it is sufficient to keep only the linear terms of Rabi frequency Ω_p in equations (1). By use of these approximations, we find the first order steady-state analytical solution for ρ_{13} can be written as

$$\rho_{13}^1 = \frac{-4A_7 + \Omega_p \{-A_1 \rho_{12}^0 + \Omega_c [-i(A_0 - A_5)p \rho_{31}^0] - 2A_2 p \rho_{13}^0 + 2A_3 \rho_{21}^0 + 2pA_6 \Omega_c \rho_{23}^0\} - 2pA_4 \rho_{32}^0}{4[-p^2 A_8 + A_{10} p^4 - 4p^6] + A_9(1 + \Delta_c^2 + 2\Omega_c^2)} \quad (3)$$

where the matrix elements ρ_{12}^0 , ρ_{13}^0 and ρ_{23}^0 are the zero order steady-state analytical solutions,

$$\begin{aligned} \rho_{12}^0 &= \frac{(-i + \Delta_p)(-2i - \Delta_c + \Delta_p)\Omega_c}{(2i + \Delta_c - \Delta_p)[p^2 + (\Delta_p - i)(\Delta_c - i)] - \Omega_c^3} \\ &\quad + (\Delta_c - i)\Omega_c^2, \\ \rho_{13}^0 &= \frac{p\Omega_c(2i + \Delta_c - \Delta_p)}{(2i + \Delta_c - \Delta_p)[ip^2 - i + \Delta_c(1 + i\Delta_p) + \Delta_p]} \\ &\quad + (1 + i\Delta_c)\Omega_c^2, \\ \rho_{23}^0 &= \frac{ip\Omega_c^2}{(2i + \Delta_c - \Delta_p)[p^2 + (-i + \Delta_p)(-i + \Delta_c)] + (-i + \Delta_c)\Omega_c^2}, \end{aligned}$$

where the parameters A_i , ($i = 0, \dots, 10$) in Eq.(3) are given in the Appendix. $\gamma_1 = \gamma_2 = \gamma$ and all the parameters are reduced to dimensionless units by scaling with γ . Using Eq.(2), which consists of both real and imaginary parts, i.e., $\chi = \chi' + i\chi''$. The imaginary part of the susceptibility gives the absorption profile of the probe field which can be written as

$$\chi'' = \frac{2N|\mu_{13}|^2}{\epsilon_0 \hbar} \text{Im}\left[\frac{\rho_{13}}{\Omega_p}\right] = \alpha \text{Im}\left[\frac{\rho_{13}}{\Omega_p}\right], \quad (4)$$

where $\alpha = \frac{2N|\mu_{13}|^2}{\epsilon_0 \hbar}$. Here we are interested in the position information of the atom via the absorption process of the probe field. Then Eq.(4) is the main result and reflects the atomic position probability distribution [6, 7]. Therefore, we can obtain the atomic position information via the corresponding parameters, i.e., the intensities of SGC and the

detunings associated with the probe and two orthogonal standing-wave fields.

NUMERICAL RESULTS AND DISCUSSIONS

2-D atom localization via the detuning Δ_p

In this following, we analyze the position information via the imaginary part χ'' of the susceptibility [6, 7]. However, the analytical expression for the position probability χ'' in Eq.(4) corresponding to the field detunings and intensities of SGC is rather cumbersome. Hence, we follow the numerical approach to get the position distribution information.

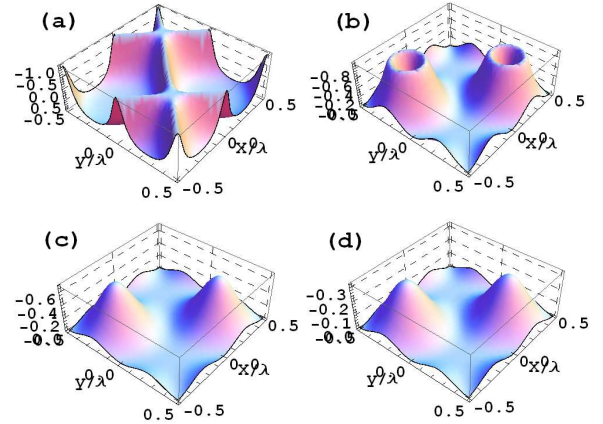


FIG. 2. (Color online) Plots for 2-D atom localization: $\text{Im}[\chi]$ as a function of (x,y) versus the probe field detuning Δ_p . (a) $\Delta_p=0$, (b) $\Delta_p=20\gamma$, (c) $\Delta_p=30\gamma$, (d) $\Delta_p=40\gamma$. The other parameters used are $\kappa_1=\kappa_2=2\pi/\lambda$, $\Omega_{c0}=10\gamma$, $\Omega_p=0.01\gamma$, $\delta=\eta=0$, $\theta=0.5\pi$, and where γ is the scaling parameter.

Initially, we consider the position information dependent the probe field detuning Δ_p . The standing-wave field is tuned to interact with the transition $|1\rangle \leftrightarrow |2\rangle$ resonantly, and $\Omega_{c0}=10\gamma$, $\Omega_p=0.01\gamma$. The position-dependent the probe detuning Δ_p is shown in Fig.2 (a) $\Delta_p=0$, (b) $\Delta_p=20\gamma$, (c) $\Delta_p=30\gamma$, (d) $\Delta_p=40\gamma$. And their density plots in Fig.2 are shown in Fig.3. As noted in Fig.2(a), the equal localization peaks distribute on the diagonal in the second and

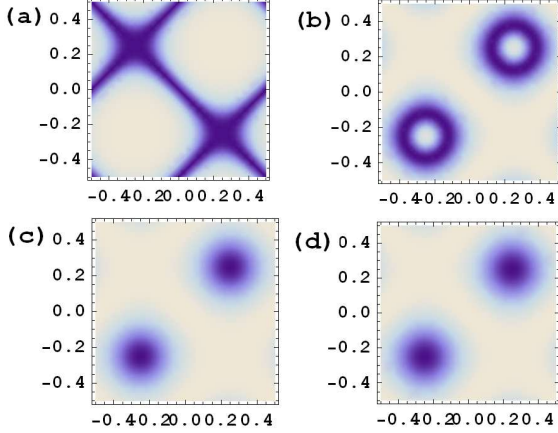


FIG. 3. (Color online) Density plots of 2-D atom localization: $\text{Im}[\chi]$ as a function of (x,y) versus the probe field detuning Δ_p . All other parameters in (a) to (d) are the same as in Figs.2(a) to 2(d), respectively.

fourth quadrants within the half wavelength [see Figs. 2(a) and 3(a)]. As the detuning Δ_p increasing, we observe the position distribution of the atom is situated in the first and third quadrants with a craterlike pattern [see Figs. 2(b)], and the atom is localized at the circular edges of the craters [see Fig. 3(b)]. Moreover, when Δ_p is tuned to an appropriate value [e.g., 30γ , 40γ in Fig. 2(c) and (d)], the position distribution displays two equivalent spikelike pattern in the quadrants I and III [see in Fig. 2(c) and (d)]. Which shows that the spatial resolution is improved via the light spots in Fig.3. These results demonstrate the increasing resolution for 2-D atom localization can be obtained by the probe detuning Δ_p .

2-D atom localization via the detuning Δ_c

Secondly, we consider the effect of the detuning Δ_c on the 2-D atom localization. Although the values of some parameters are the same as in Fig. 2, the behavior of the atom localization in Fig.4 is different from those in the previous subsection. Similarly, the corresponding density plot

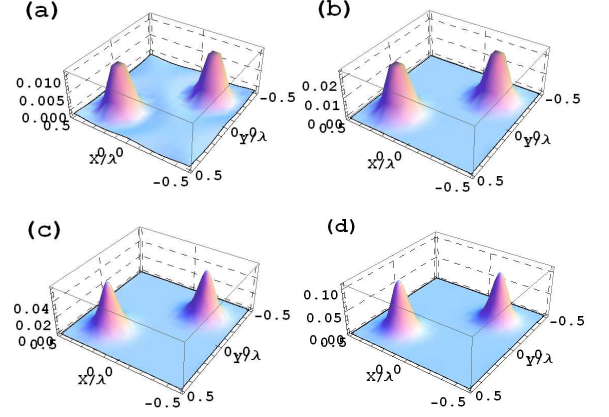


FIG. 4. (Color online) Plots for 2-D atom localization: $\text{Im}[\chi]$ as a function of (x,y) versus the coupled standing-wave field detuning Δ_c . (a) $\Delta_c=8\gamma$, (b) $\Delta_c=12\gamma$, (c) $\Delta_c=15\gamma$, (d) $\Delta_c=20\gamma$. All other parameters are the same as in Fig.2.

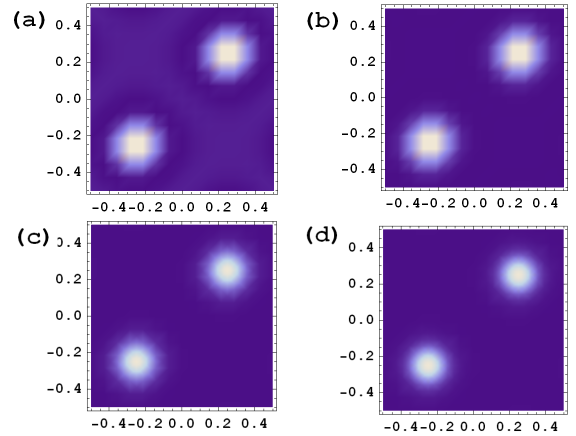


FIG. 5. (Color online) Density plots of 2-D atom localization: $\text{Im}[\chi]$ as a function of (x,y) versus the probe field detuning Δ_c . All other parameters in (a) to (d) are the same as in Figs.4(a) to 4(d), respectively.

of Fig.4 is given in Fig.5. When the detuning of two orthogonal standing-wave fields is set as 8γ in Figs.4 (a), 12γ in Figs.4(b), 15γ in Figs.4(c) and 20γ in Figs.4(d) with the probe field coupling the atomic system off-resonantly, i.e. $\Delta_p=20\gamma$, two spikelike patterns with equal increasing peak maxima occur in the quadrants I and III of the x - y plane. And their peak values increase from 0.01 to 0.1. Meanwhile, the spikelike structure become more and more

acuity, and the dual light-spot size in Fig.5 confirms these straightly. As a result, we can achieve an increasing precision resolution for 2-D atom localization by measuring the detuning Δ_c under the condition of the probe field coupling the atomic system off-resonance. Then an increasing resolution for 2-D atom localization can be obtained by the above two different detunings.

2-D atom localization via the intensities of SGC

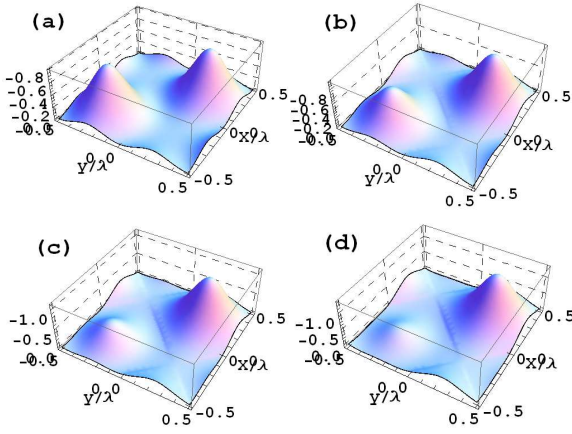


FIG. 6. (Color online) Plots for 2-D atom localization: $\text{Im}[\chi]$ as a function of (x,y) versus the intensities p of SGC. (a) $\theta = \pi/1.99$, (b) $\theta = \pi/1.9$, (c) $\theta = \pi/1.8$, (d) $\theta = \pi/1.7$. $\Delta_c=0$, $\Delta_p=30\gamma$. All other parameters are the same as in Fig.2.

As a matter of fact, we are particularly interested in the influence of the intensities $p=\cos\theta$ of SGC on the behavior of 2-D atom localization, we give the 2-D localization dependent the intensities $p=\cos\theta$ of SGC, where $\cos\theta$ depicting the intensities of SGC is set as (a) $\theta=\pi/1.99$, (b) $\theta=\pi/1.9$, (c) $\theta=\pi/1.8$, (d) $\theta=\pi/1.7$ in Fig.6. The corresponding density plots are illustrated in Fig. 7. For the sake of simplification, we set the standing-wave field drives the transition $|1\rangle \leftrightarrow |2\rangle$ resonantly, i.e, $\Delta_c=0$, and $\Delta_p=30\gamma$. All other parameters are the same as in Fig.2.

As noted In Fig.6(a), two spikelike patterns with the

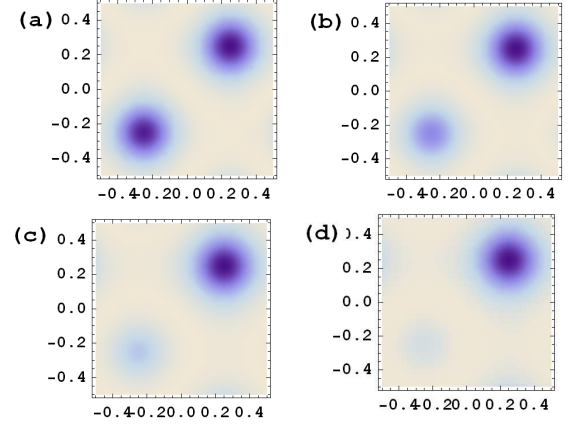


FIG. 7. (Color online) Density plots of 2-D atom localization: $\text{Im}[\chi]$ as a function of (x,y) versus the intensities p of SGC. All other parameters in (a) to (d) are the same as in Figs.6(a) to 6(d), respectively.

equal peak maxima(-0.8) appear in the first and third quadrants[also see Figs.7(a)]. When the θ corresponding to the intensity of SGC is detected at $\pi/1.9$, the peak maxima in quadrant III decreases while the other one in quadrant I remains, which shows the probability of the atom distributing in the third quadrant decreases [see Figs.6(b) and 7(b)]. For the case of $\theta=\pi/1.8$, the single-spikelike pattern is distributed in the first quadrant and very few in the third quadrant, as can be seen Figs.6(c) and Figs.7(c). Continuing to adjust $\theta=\pi/1.7$, there's almost zero peak distribution in the third quadrant [see Figs.6(d) and 7(d)], which demonstrates the spatial resolution of atomic position is greatly improved. The identical multi-peak scheme for 2-D localization has the disadvantage that it is unknown which one is responsible for a possible atomic position distribution. However, one can determine more precisely where the atoms is via the single-peak position distribution. So, a better resolution can achieved by the tuned intensities p of SGC than by the previous detunings.

CONCLUSION

In summary, the roles of SGC and detunings associated with the probe and two orthogonal standing-wave fields in the 2-D atom localization were investigated in our scheme. Two equal and flexibly tunable localization peaks for the 2-D atom localization are observed when the detunings were tuned. However, when the intensities of SGC were manipulated, two peaks with one increasing and other decreasing are observed, and finally the single-peak is shown in the x-y plane. The single-peak for 2-D atom localization has more advantage than the multi-peak case because of the determining atomic position more precisely via the single localization peak. So, the advantage in 2-D atom localization via both the external fields and the quantum coherence is obtained in our scheme.

appendix

$$\begin{aligned}
A_0 &= P^4(8i + \Delta_c - 3\Delta_p) + \Omega_c^2(5i + \Delta_c - 2\Delta_p)[\Omega_c^2 \\
&\quad + (i + \Delta_p)(-2i + \Delta_c - \Delta_p)] + P^2[(i + \Delta_p) \\
&\quad (i + \Delta_c)(8i + \Delta_c - 3\Delta_p) + 2\Omega_c^2(5i + \Delta_c - 4\Delta_p)], \\
A_1 &= 2iP^2\{(8i + \Delta_c - 3\Delta_p)[P^2 + (i + \Delta_p)(i + \Delta_c)] + \Omega_c^2 \\
&\quad (4i + \Delta_c - 3\Delta_p)\}, \\
A_2 &= 2P^4 - [\Omega_c^2 + (i + \Delta_p)(-2i + \Delta_c - \Delta_p)] \\
&\quad [\Omega_c^2 + (i + \Delta_c)(-3i + \Delta_p)] + P^2[4 + \Omega_c^2 + \\
&\quad \Delta_p(i + \Delta_p) + \Delta_c(5i + \Delta_p)], \\
A_3 &= -iP^4(-4i + \Delta_c - 3\Delta_p) + 2[\Omega_c^2 + (i + \Delta_p)(-2i + \Delta_c \\
&\quad - \Delta_p)](1 + \Delta_c^2 + 2\Omega_c^2) - iP^2\{\Delta_p(5 - 3i\Delta_p) \\
&\quad + \Delta_c^2(3i + \Delta_p) + \Omega_c^2(2i - 3\Delta_p) + \Delta_c[9 - \Delta_p \\
&\quad (8i + 3\Delta_p) + \Omega_c^2]\}, \\
A_4 &= 8iP^4 + P^2\{-2i[8 + \Delta_c(-4i + \Delta_c) - 4i\Delta_p - 6\Delta_c\Delta_p \\
&\quad + \Delta_p^2] + \Omega_c^2(6i + \Delta_c - 5\Delta_p)\} + [\Omega_c^2 \\
&\quad + (i + \Delta_p)(-2i + \Delta_c - \Delta_p)][2(1 - i\Delta_c)(2i + \Delta_c - \Delta_p) \\
&\quad + \Omega_c^2(3i + \Delta_c - 2\Delta_p)],
\end{aligned}$$

The parameters A_i in Eq.(3) are given by the following:

$$\begin{aligned}
A_5 &= P^4(4i + \Delta_c - 3\Delta_p) + [\Omega_c^2 + (i + \Delta_p)(-2i + \Delta_c - \Delta_p)] \\
&\quad [2(i + \Delta_c)(3 + i\Delta_p) + \Omega_c^2(7i + \Delta_c - 2\Delta_p)] + P^2\{\Delta_c^2 \\
&\quad (i + \Delta_p) + \Delta_p(-3 - 5i\Delta_p - 8\Omega_c^2) + 8i(-2 + \Omega_c^2) + \Delta_c \\
&\quad [1 + (4i - 3\Delta_p)\Delta_p + 2\Omega_c^2]\}, \\
A_6 &= P^2(6i + \Delta_c - 5\Delta_p) + (5i + \Delta_c - 2\Delta_p)[(-2i + \Delta_c \\
&\quad - \Delta_p)(i + \Delta_p) + \Omega_c^2], \\
A_7 &= -4iP^5\Omega_c + iP^3[8 + \Delta_c^2 + \Delta_p(-4i + \Delta_p) - 2\Delta_c(2i + 3\Delta_p)] \\
&\quad [\Omega_c + p\Omega_c[(2 + i\Delta_c - i\Delta_p + i\Omega_c^2)(i + \Delta_p)][(i + \Delta_c) \\
&\quad (2i + \Delta_c - \Delta_p) + \Omega_c^2] + (1 + \Delta_c^2 + 2\Omega_c^2) + \{[4 + (\Delta_c \\
&\quad - \Delta_p)^2](i + \Delta_p) + (2i + \Delta_c - \Delta_p)\Omega_c^2\}\Omega_p + P^2 \\
&\quad \{(\Delta_c - i)[8 + \Delta_c]^2 + \Delta_p(\Delta_p - 4i) - 2\Delta_c(2i + 3\Delta_p)\} \\
&\quad - [12i + 5\Delta_c + (3 + 2i\Delta_p)\Delta_p]\Omega_c^2 - i\Omega_c^4\}\Omega_p \\
&\quad + 2P^4[-2\Delta_c + i(2 + \Omega_c^2)]\Omega_p, \\
A_8 &= -2\Delta_c^3\Delta_p + 6(2 + \Delta_p)^2 - 2\Delta_c\Delta_p(6 + \Delta_p)^2 \\
&\quad + \Delta_c^2(6 + 8\Delta_p)^2 + 2[4 - (\Delta_c - 4\Delta_p)(\Delta_c + \Delta_p)] \\
&\quad \Omega_c^2 + \Omega_c^4, \\
A_9 &= [4 + (\Delta_c - \Delta_p)^2](1 + \Delta_p)^2 + 2[2 + (\Delta_c - \Delta_p)\Delta_p] \\
&\quad \Omega_c^2 + \Omega_c^4, \\
A_{10} &= 12 + \Delta_c^2 - 10\Delta_c\Delta_p + \Delta_p^2 - 4\Omega_c^2.
\end{aligned}$$

- [2] W. D. Phillips, Rev. Mod. Phys. **70** 721 (1998).
- [3] S. Qamar, S. Y. Zhu and M. S. Zubairy, Phys. Rev. A **61** 063806 (2000).
- [4] S. Qamar, S. Y. Zhu and M. S. Zubairy, Opt. Commun. **176** 409 (2000).
- [5] J. Xu and X. M. Hu, Phys. Lett. A **366** 276 (2007).
- [6] M. Sahrai, H. Tajalli, K. T. Kapale and M. S. Zubairy, Phys. Rev. A **72** 013820 (2005).
- [7] K. T. Kapale and M. S. Zubairy, Phys. Rev. A **73** 023813 (2006).
- [8] E. Paspalakis and P. L. Knight, Phys. Rev. A **63** 065802 (2001).
- [9] C. P. Liu, S. Q. Gong, D. C. Cheng, X. J. Fan and Z. Z. Xu, Phys. Rev. A **73** 025801 (2006).
- [10] D. C. Cheng, Y. P. Niu, R. X. Li and S. Q. Gong, J. Opt. Soc. Am. B **23** 2180 (2006).
- [11] G. S. Agarwal, and K. T. Kapale, J. Phys. B **39** 3437 (2006).
- [12] J. Xu and X. M. Hu, Phys. Rev. A **76** 013830 (2007).
- [13] S. Kunze, K. Dieckmann and G. Rempe, Phys. Rev. Lett. **78** 2038 (1997).
- [14] R. Quadt, M. Collett and D. F. Walls, Phys. Rev. Lett. **74** 351 (1995).
- [15] S. Qamar, A. Mehmood and S. Qamar, Phys. Rev. A **79** 033848 (2009).
- [16] V. Ivanov and Y. Rozhdestvensky, Phys. Rev. A **81** 033809 (2010).
- [17] R. G. Wan, J. Kou, L. Jiang, Y. Jiang and J. Y. Gao, J. Opt. Soc. Am. B **28** 622 (2011).
- [18] C. Ding, J. Li, X. Yang, D. Zhang and H. Xiong, Phys. Rev. A **84** 043840 (2011).
- [19] Rahmatullah and S. Qamar, Phys. Rev. A **88** 013846 (2013).
- [20] O. Kocharovskaya, A. B. Matsko and Y. Rostovtsev, Phys. Rev. A **65** 013803 (2001).
- [21] P. Meystre, M. Sargent III, Elements of Quantum Optics, 3rd ed. (Springer-Verlag, Berlin, 1999).
- [22] S. Menon and G. S. Agarwal, Phys. Rev. A **61** 013807 (1999).

* Supported by the National Natural Science Foundation of China (Grant Nos. 61205205 and 6156508508), the General Program of Yunnan Provincial Research Foundation of Basic Research for application, China (Grant No. 2016FB009) and the Foundation for Personnel training projects of Yunnan Province, China (Grant No. KKSJ201207068).

† Corresponding author: zhaosc@kmust.edu.cn

[1] P. Storey, M. Collett, Phys. Rev. A **47**, 405 (1993).